Hue discrimination, unique hues and naming

Romain, Bachy[1]; Jérôme, Dias[2,3]; David, Alleysson[3];Valérie, Bonnardel[1*]

[1]*Department of Psychology, The University of Winchester, Winchester, SO22 4NR, United Kingdom*

[2]*Laboratoire de Caractérisation des Systèmes Photoniques, CEA-LETI, Grenoble, France*

[3]*Laboratoire de Psychologie et Neurocognition, Université Pierre Mendès France, Grenoble, 38000, France*

[*]*Corresponding : Valerie.Bonnardel@winchester.ac.uk*

The Hue Discrimination Curve (HDC) that characterizes performances over the entire hue circle was determined by using Sinusoidally Modulated Spectral Power Distributions of 1.5 c/300 nm with fixed amplitude and twelve reference phases. To investigate relationship between hue discrimination and appearance, observers further performed a free color naming and a unique hue tasks. The HDC consistently displayed two minima and two maxima; discrimination is optimal at the yellow/orange and blue/magenta boundaries and pessimal in green and in the extra-spectral magenta colours. A linear model based on Müller zone theory correctly predicts a periodical profile but with a phase-opponency (minima/maxima at 180° apart) which is inconsistent with the empirical HDC's profile.

Keywords: Hue Discrimination Curve, Color naming, Unique Hues, Sinusoidal Spectral Power Distributions.

OCIS codes: 330.1720,330.4060,330.5510

[1]

---

[1] The paper is published as Romain Bachy, Jérôme Dias, David Alleysson, and Valérie Bonnardel, *"Hue discrimination, unique hues and naming,"* **J. Opt. Soc. Am. A** 29, A60-A68 (2012) http://www.opticsinfobase.org/abstract.cfm?URI=josaa-29-2-A60

1. Introduction

A defining aspect of categorical perception is the existence of "[$\cdots$] a quantitative discontinuity in discriminability at the category boundaries of a physical continuum, as measured by a peak in discriminative acuity at the transition region for identification of members of adjacent categories." [1]. This definition, applied to categorical perception of colors, suggests that color category boundaries perceived in a continuous color spectrum are associated with regions of optimal discrimination. Experience shows that when subjects are either imposed a fix number of six delineations (thin black lines perpendicular to the direction of color variation in the spectrum) [2] or freely choose the number of delineations to mark their perceived color category boundaries in a diffracted spectrum [3], although the large inter-observer variation in the judgments, seven color categories are commonly reported among English and American subjects. These categories are identified by Smeulders et al. (1994) [2] subjects as violet, blue turquoise, green, yellow, orange and red. Category boundaries vary across subjects, but a rough average estimate provides locations at 470, 490, 510, 575, 595 and 610 nm. Yet the discrimination minima approximately located at 440, 490 and 590 nm in the wavelength discrimination curve [4] do not provide a convincing argument on the expected relationship between region of optimal discrimination and localization of perceived category boundaries.

More recently, Danilova & Mollon (2010) [5] took the opposite stance and investigated the possibility of a discrimination enhancement at the frontier between two binary hues such as chartreuse (yellow-green) and orange (yellow-red) which corresponds to the point of subjective unique hue (i.e. phenomenologically unmixed color). In their experiment, CRT monitor stimuli were defined in terms of cone excitation ratios and were chosen to lie on 45°-segments crossing the line of approximate unique blue (476 nm) and approximate unique yellow (756 nm). Results indicate that, within the set of stimuli tested, relative discrimination minima were located close to the unique hue loci for the region of lesser saturation, and unique hue loci and discrimination minima could be plotted on lines running parallel to the blue-yellow unique hue line.

An earlier study from Holtsmark & Valberg (1969) [6] also addressed the possibility of a correlation between discrimination and unique hues. For this purpose, the authors used a Spectral Colour Integrator offering the facility to produce rectangular masks that could be applied onto a prismatic spectrum. Their rectangular masks of different bandwidths corresponded to optimal colors. This system allowed discrimination to be probed in non-spectral regions. Maxima of discrimination were found in the green and magenta regions. One minimum was reported for a near-monochromatic yellow (576 nm) and two other minima, although at different purity levels, coincided with lines of unique blue and unique red determined from the averaged setting of four observers. A forth relative minima was reported in blue-green region.

In the present experiment, we use Sinusoidally modulated Spectral Power Distributions (SSPDs) to address the question of the relationship between discrimination and perceived hues. For this study, SSPDs show several advantages compared to either monochromatic lights or to a mixture of three primary lights. SSPDs, at the time designed as comb-filtered spectra, were first introduced in the field of color vision by Horace Barlow [7]. From an information theory perspective, the initial purpose of their use in the study of color was to address the question of color dimensionality [8]. It has been then subsequently shown that SSPDs could be considered as idealized models of natural color signals [9] and, compared to monochromatic lights, SSPDs offer a more ecologically valid stimulus. Indeed, Mizokami et al. (2006) [10], using gaussian spectra of variable bandwidths, revisited the interpretation of Abney's effect obtained with a mixture of monochromatic light and white light and concluded that wavelength changes observed under these later conditions were attributable to the compensation for eye's spectral filtering that is normally applied with natural broadband color signals. A second advantage of SSPDs is no prior knowledge of observer cone-fundamental is necessary. Individual differences in ocular media and spectral photopigments introduce translation and rotation of the discrimination axis in a chromaticity diagram compared to the nominal axis which might have implications in stimulus specifications based on a set of cone-fundamentals [11]. Finally, SSPDs have the interesting colorimetric property, that for constant frequency and amplitude, their chromaticities lie on a perfect elliptical contour when phase varies from 0 to 360°. This property holds true for any chromaticity diagram and for any broadband light source over which the sinusoidal modulation applied. Thus phase, as a parameter of the physical stimulus, conveniently bridges the spectral interval with the color circle.

2. Method

2.A. Observers

Two of the authors (VB & RB) participated in the experiment. Both have a normal trichromatic color vision as assessed by Ishihara Isochromatic plates (24 plates) and the Farnsworth-Munsell 100 hue test.

2.B. Apparatus

A light stimulator fully described elsewhere [12] was used to produce SSPDs. Briefly, it comprises a 150 W xenon light source illuminating a linear interference wedge yielding a continuous spectrum from 400 to 700 nm that is linear in wavelength units. The light is then transmitted through a black and white LCD panel (adapted Apple Macintoch Powerbook Duo 280) and recollimated into an integrating sphere. Through a simple Maxwellian system, observers see monocularly the aperture of the integrating sphere which produces a homogeneous 2° spot of absolute estimated luminance of $5 - 6$ cd/m^2. A white cardboard panel illuminated by a 50 W halogen lamp equipped with daylight filters provides a background of 4 cd/m^2 with CIE 1931 chromaticity coordinates of (0.359, 0.335) (see Fig. 1).

2.C. Stimuli

The LCD panel acts as an electronic mask imposing sinusoidal modulations directly applied to the interference wedge. The resulting illumination, noted $SPD_\varphi(\lambda)$ can be expressed by the following equation (see App. A for details):

$$\begin{aligned} SPD_\varphi(\lambda) &= A(\lambda)E_0(\lambda)(E_\varphi(\lambda) - 1) + E_0(\lambda) \\ \text{with} & \\ E_\varphi(\lambda) &= 1 + m\sin(p(f(1.2\lambda + 480) + \varphi)) \end{aligned} \tag{1}$$

$E_\varphi(\lambda)$ is the modulation function; $E_0(\lambda)$ the spectral power distribution in absence of modulation; $A(\lambda)$ the gain function, m amplitude of modulation (varying from 0 to 1); f the frequency (cycles per 300 nm, noted c) and φ_0 the initial phase which by convention is equal to 0° when for a maximal modulation the sinusoid increases from the mean level of modulation at the 400 nm end, where $p = \pi/180$ scales the spectral interval in a $0 - 360°$ interval. Sinusoidal modulations were displayed at the maximum of amplitude ($m = 1$) with a constant frequency equal to 1.5 c. A set of twelve reference phases was tested (0-30-80-90-100-150-180-210-240-270-330 and 345°).

2.D. Light measurements

All spectral measurements were performed with an Ocean Optic spectrometer (S2000). The light spot SPD was measured at the output of the integrating sphere with the spectrometer directly fitted to one of its aperture. The background illuminant SPD was measured by pointing the spectrometer on the cardboard panel 1 cm away from the light spot. Chromaticity coordinates were computed from SPD measures. As previously reported, for a given frequency with a constant amplitude, chromaticity coordinates of SSPDs vary along an ellipse in a chromaticity diagram when phase changes from 0 to 360° [12, 13]. The elliptical contour fitted to the chromaticities of our measured SSPDs is plotted in Fig. 1.

From this set of spectral measurements, we derived a model allowing us to determine the SPDs for our experimental conditions (see App. A). These computed SSPDs were used in the chromaticity coordinate computation for any phase φ in our experimental condition, in Fig. 1, Fig. 3 and in subsequent modeling (see Sec. 4.B).

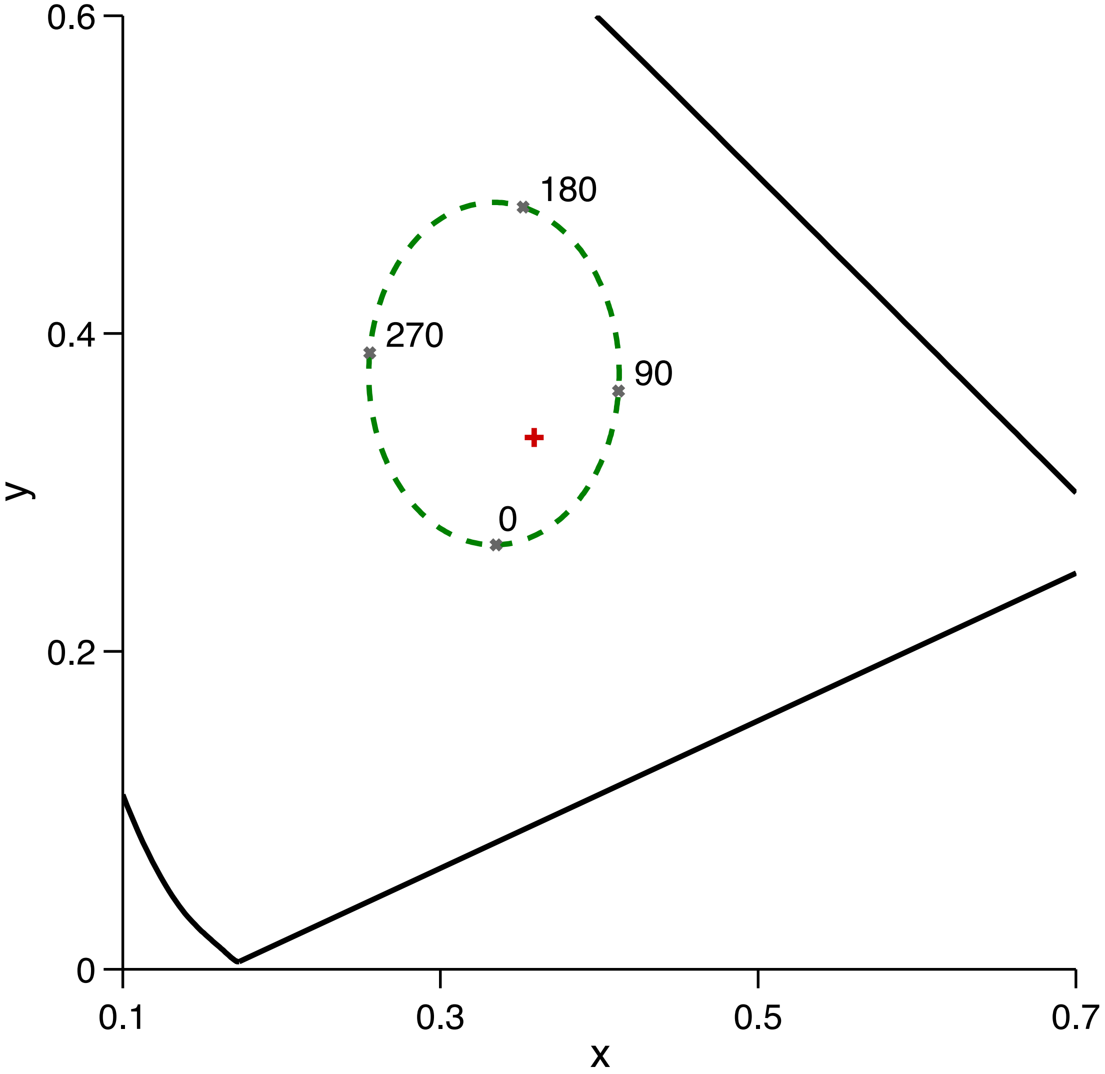

Fig. 1. (Color online) Chromaticity coordinates of our stimuli plotted in the CIE 1931 diagram lie on an elliptical contour (dashed line) when phase varies from 0 to 360°. Empirical measures of the sinusoidally modulated spectra are shown in App. A (Fig. A(b)). The locus of background illuminant is indicated by the cross.

2.E. Procedure

Discrimination task: Observer had their head resting on a chinrest. In a three-alternative temporal forced choice, a reference phase (φ) appeared twice and a test phase ($\varphi + \delta\varphi$) appeared once in the three temporal window (500 ms) in a random fashion. The task was to indicate which stimulus differed from the other two by pressing one of the three response keys. To ensure that brightness could not be used as a cue, the program introduced luminance variations of ranging from 1:1.25 by applying patterns to the electronic mask in a random fashion. Between stimuli presentation the electronic mask was in off state with a luminance level below 1 cd/m^2. The just noticeable phase difference ($\Delta\varphi$) was determined by an adaptive staircase procedure. The initial value of $\delta\varphi$ was set at 10°, after three positive answers it was reduced by 1°, and increased by 1° after one negative answer. Three interleaved staircase procedures run in parallel and terminated after ten reversals and the last five reversals were used for threshold computation. For each reference phase, a minimum of three determinations were performed and averaged to compute the threshold.

Unique Hue task: Using standard estimates of unique blue (476 nm), unique yellow (576 nm), unique green (545 nm) and unique red (c489 nm) as starting points [5, 14, 15], a set of corresponding phases on each side of these estimates were presented in a random fashion. Each unique hue was tested individually. To define the range of test phases around the estimated unique hue, the testing session started by the presentation of extreme phase values eliciting a non-ambiguous answer. This interval was subsequently reduced in a step-by-step iterative process. A minimum of four stimulus presentations were made for critical values. For each stimulus presentation, observer had to decide if the stimulus was 'greenish', 'reddish' or 'neither' for unique yellow and unique blue, or 'bluish', 'yellowish' or 'neither' for unique red and unique green. The determined unique hue corresponded to phases for which the observer's answer was either systematically alternated, or corresponded to the central value of an interval eliciting neither responses. After each presentation, observers remove their eye from the eye-piece to avoid uncontrolled stimulation while the experimenter was changing the stimulus. No time constraint applied to this task.

Naming task: Observers were presented with twelve stimuli corresponding to reference phases ranging from 0 to 330 in 30° step. In RBs case, a supplementary stimulus corresponding to one of the minima of discrimination (namely 100°) was also tested for naming. Hence for the two observers colour names were collected at regular phase step around the hue circle and included observers minima and maxima of discrimination. For each stimulus, observers were requested to name the colour in a free naming task. Stimuli were presented in random fashion, after each presentation observers closed their eye awaiting for the next stimulus presentation. No time constraint applied to this task.

3. Results

3.A. *Hue discrimination curve*

The experimental hue discrimination curve (HDC) ($\Delta(\varphi)/\varphi$) shows a similar profile for the two observers with RB exhibiting an overall higher absolute sensitivity compared to VB (see Fig. 2). The curve is characterized by two minima located at 330° (VB and RB) and at 90° (VB) & 100° (RB) and by two maxima at 30° (VB and RB) and 180° (VB) & 210° (RB).

For comparison with Wright and Pitt (1934) wavelength discrimination curve ($\Delta(\lambda)/\lambda$) [4], SSPDs dominant wavelengths (λ_d) for minima and maxima were graphically determined taking the background illuminant as the achromatic stimulus. The first HDC minimum situated at 330° with a λ_d at 478 nm is slightly shifted toward shorter wavelengths compared to the $\Delta(\lambda)/\lambda$ 490 nm minimum. The λ_d determined for the second minima at 90° (VB) & 100° (RB), are respectively equal to 586 & 580 nm and are also shifted towards shorter wavelengths compared to the $\Delta(\lambda)/\lambda$ 590 nm minimum. The poor discrimination observed at 180° (VB) & 210° (RB) with dominant wavelengths of 555 & 534 nm respectively correspond to the region of poor discrimination on the $\Delta(\lambda)/\lambda$ curve with a peak situated at 530 nm. The second maximum located at 30° that could not be determined with monochromatic lights is situated on the alychne with a complementary wavelength at c542 nm.

3.B. *Unique Hues*

For comparison purposes, phases corresponding to unique hues are reported on the HDC in Fig. 2. A good inter-observer agreement is obtained for the loci of unique red, 79° (VB) vs. 76° (RB), unique yellow, 122° (VB) vs. 117° (RB) and unique blue at 317° (VB) vs. 320° (RB), and a discrepancy is observed for the unique green located at 220° for VB and at 196° for RB. While for both observers, no unique hue determination coincides with a minimum of discrimination, unique red and unique blue are situated in a region of good discrimination whereas unique green belongs to a region of poor discrimination and RB unique yellow is located in a region of relatively good discrimination.

In Fig. 3, phases corresponding to unique hues and phases eliciting minima and maxima of discrimination are plotted in the CIE 1931 chromaticity diagram. For both observers, unique yellow and unique blue loci lie in close proximity to the blue-yellow line (476 nm - 576 nm). Unique blue is located in the vicinity of a minimum of discrimination, but unique yellow is situated at some distance from the second minima. VBs second discrimination minimum is close to her unique red loci, whereas RBs second minimum is situated between his unique yellow and unique red.

Unique yellow λ_d is equal to 574 nm (VB) and 576 nm (BR), unique blue λ_d is equal to 484.5 nm (VB) and 484 nm (BR), unique red λ_d is equal to 599 nm (VB) and 619 nm (BR) and unique green λ_d is equal to 529 nm (VB) and 550 nm (BR).

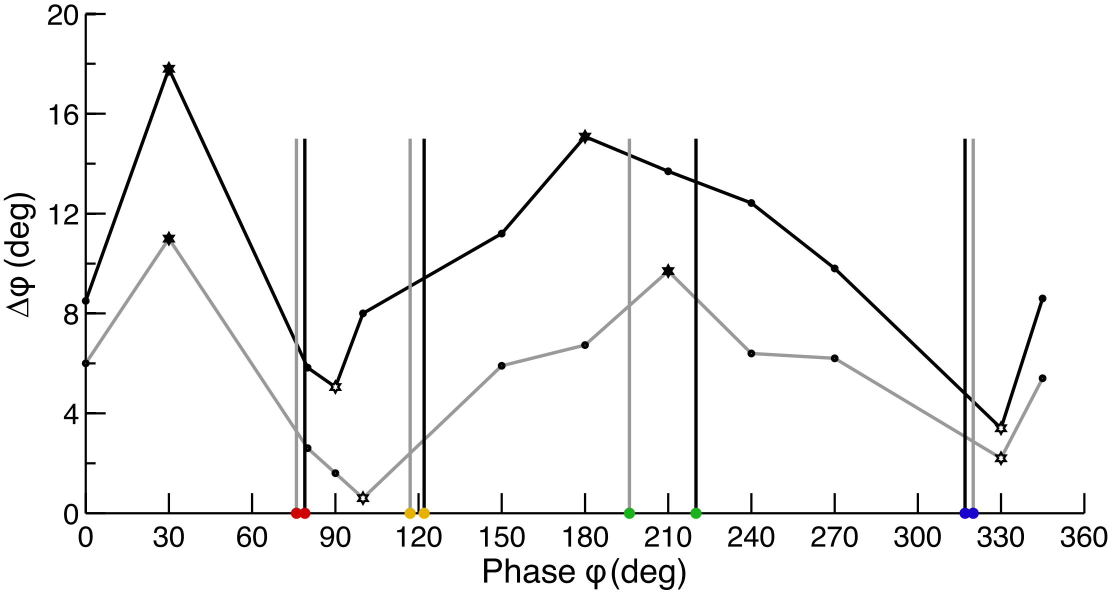

Fig. 2. (Color online) Thresholds $\Delta(\varphi)$ are plotted in function of the reference phase φ for observers VB (black line) and RB (grey line). Minimal thresholds (empty symbols) are located at 330° for the two observers and at 90 and 100° for VB and RB respectively. Maximal threshold (filled symbols) are located for the two observers at 30° and at 180° and 210° for VB and RB respectively. Vertical bars indicate the location of unique hues at 79, 122, 220 and 317° for VB and 76, 117, 196 and 320° for RB.

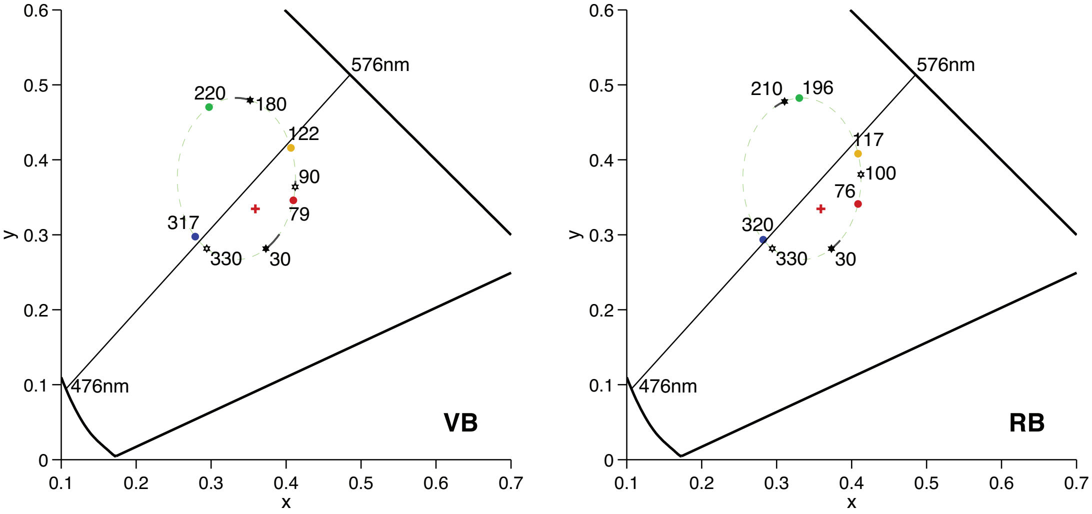

(a) (b)

Fig. 3. (Color online) For each observer, a section of the CIE 1931 diagram showing minimum (empty symbols) and maximum (filled symbols) of discrimination, and unique hue (plain circles) loci together with the line that runs from approximately unique yellow (576 nm) to approximately unique blue (476 nm). For the two observers, unique yellow and unique blue are in close proximity with the unique hue line.

3.C. Color Naming

Data from the color naming task are reported in Fig. 4 on a color circle in which hues corresponding to 10° steps were simulated taking into account our background illuminant. Note that this color circle has no bearing on perceptual order system such as the Munsell Color System, but directly relies on the physical stimuli characteristic to provide a SSPD color circle representation for our experimental conditions.

VB and RB color names follow the P-R-O-Y-YG-G-BG-B (P: purple, O: orange) order of unique and binary hues and are consistent with the simulated colors as displayed on a sRGB monitor.

Reference phases corresponding discrimination minima are described as a mixture of blue (330°) or yellow (90 & 100°) with a tiny tinge of red. At 330°, VB describes the stimulus as blue with a tinge of red and RB as blue purple. Thresholds were obtained while phase shift induced a change of hue in the direction of magenta colors, thus corresponding to a red component increase. At 90°, VB names the color as light peach and RB describes the 100° corresponding to his minima as off white pink. In this case, thresholds were obtained when the red component was decreased; the phase shift produced change of hue moving towards observers unique yellow. Maxima of discrimination correspond to colors described as binary hues. At 30°, the stimulus is described as pink (VB) and magenta (RB). At 180°, it corresponds to a green lime (VB) and at 210° to a jade color (RB).

Despite $150-270°$ corresponding to an interval of poorer discrimination, it is worth noting subjects consistency between their color naming and their unique green locus. At 180°, VB's naming (green lime) is indicative of her perception of a yellow component well into the green category where RB reports a green color. Conversely, at 210° RB's naming (jade) reflects his perception of a blue component whereas it is not until 270° that VB's naming is indicative of a blue component (green turquoise). Consistent with their naming patterns and compared to each other, RB's unique green (196°) includes a more prominent yellow component whereas VB's unique green (220°) includes a stronger blue component.

4. Discussion

4.A. Empirical hue discrimination curve

SSPDs HDC provides a characterization of discrimination performances over the entire hue circle including the magentas that are absent from the wavelength discrimination curve. A comparison between the two curves requires the SSPDs λ_d determination that critically depends on the achromatic point and a word of caution should be given here. In Sec. 3, we used the background illuminant as the achromatic point. However, this point might not fully specify the state of adaptation of the eye at the stimulation retinal location since between stimuli presentations the LCD was offset and produced a dim spot (below 1 cd/m^2) for

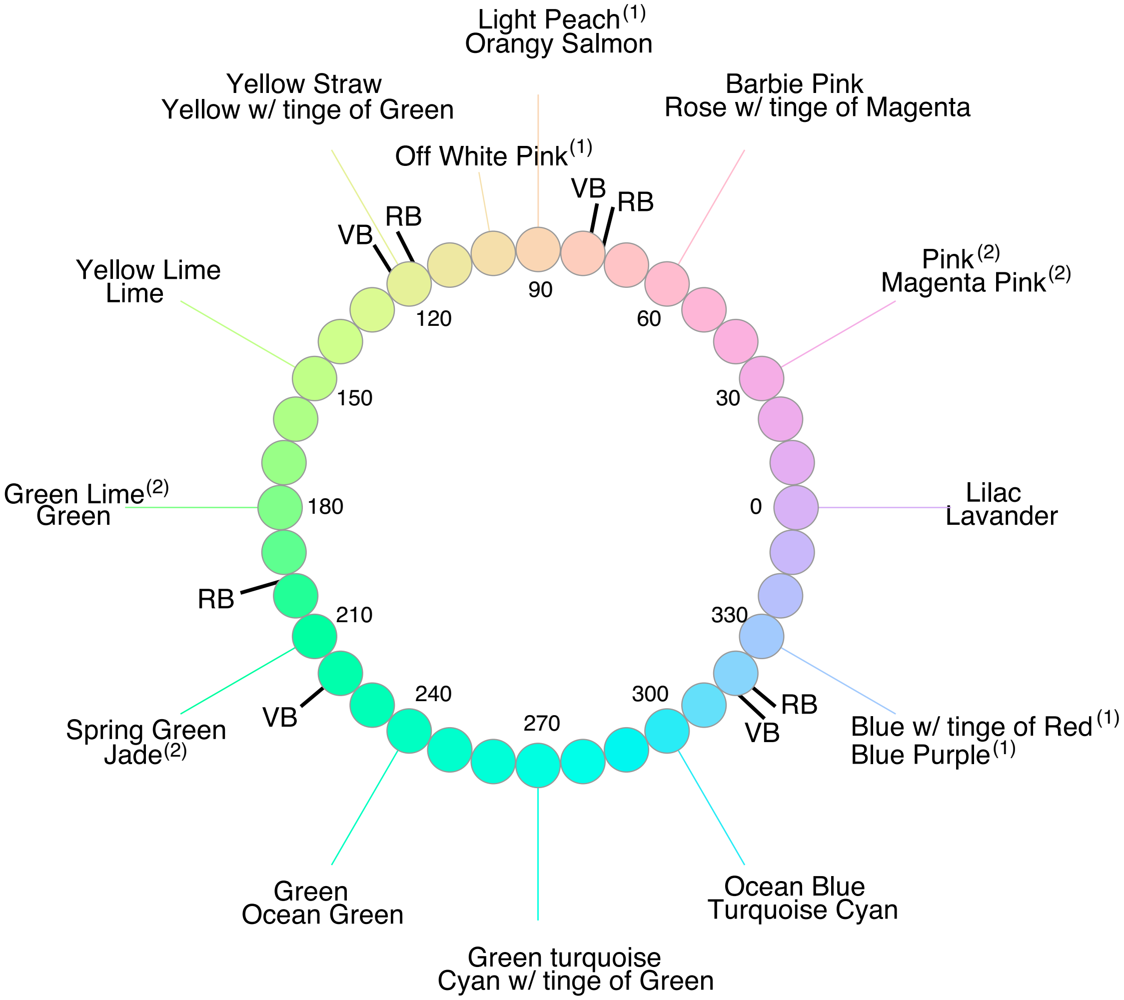

Fig. 4. (Color online) Hue circle obtained from simulated hues corresponding to a 10° phase-step. This simulation, valid for a sRGB color space display, takes into account the background illuminant of our experimental condition. Color names for 12 stimuli in 30° step are reported for VB (top) and RB (bottom). An additional color name is reported for RBs optimal discrimination at 100°. Thick black lines indicate the unique hue loci. Minima (1) and maxima (2) of discrimination elicit names corresponding to binary hues.

500 ms. This caution should be kept in mind when we refer to SSPDs λ_d.

In summary and for SSPDs phases tested, the HDC profile is clearly characterized by two minima and two maxima. VB's and RB's maxima (180 & 210°) observed in the green region and respectively identified as 'green lime' and 'jade' are in good agreement with the region of poorer discrimination around 530 nm shown on the wavelength discrimination curve and with the maxima reported to lie along the line of unique green by Holtsmark and Valberg (1969) [6] with optimal colour stimuli. The second maximum (30°) consensual for the two observers and identified as 'pink' and 'magenta pink' corresponds to a colour with a complementary wavelength (c542 nm) situated on the alychne and is in good agreement with the poor discrimination performances reported in magentas (around c525 nm) by Holtsmark and Valberg (1969) [6].

The first minimum at 330° consensual for the the two observers and identified as 'blue with tinge of red' and 'blue purple' is close to minima reported in a direction identified as the unique blue curve and associated to the $\Delta(\lambda)/\lambda$ deep blue minimum located at 440 nm in Holtsmark and Valbergs' results [6]. The second minimum at 90° (VB) or 100° (RB) identified as 'light peach' or 'off white pink' is less readily correlated with previous reports. These minima located between VB's and RB's unique yellow and unique red settings with a bias towards unique red (especially in VB's case) could correspond to discrimination minima located on Holtsmark and Valbergs unique red line [6].

Based on naming data and on SSPDs λ_d, the HDC two minima are thus in closer agreement with discrimination minima determined with optimal colors and located on unique blue and unique red curve, than those reported for monochromatic yellow and blue-green in the wavelength discrimination curve. Indeed, these later minima, also present in Holtsmark and Valberg (1969) [6] results, occurred for near-monochromatic yellow and blue-green stimuli, that is for a higher saturation level than those that could be produced with SSPDs.

4.B. Computational model

Due to our stimuli characterization as sinusoidal modulations of spectral energy, the HDC can be modeled by simple computation steps. For a given frequency and a constant level of modulation, SSPDs physical energy is fully defined by two independent variables: λ and φ. A signal modulation exclusively induced by a phase φ variation, $(\delta\varphi)$ is described by a sinusoidal function which has the convenient properties to be continuous and differentiable. In a first step, using Eq. 1 derived from the SSPDS measurements we are able to compute any SSPDs used in our experimental conditions (see App. A for computation details).

In a second step we computed visual responses to SSPDs. It can be shown (see App. B and also [16]) that responses of a set of cone-fundamentals to phase variation φ are sinusoidal functions (see Fig. B). Likewise, responses of color opponent mechanisms responses which are linear combination of cone-fundamentals are sinusoidal functions (see App. B and Fig. C). Sensitivity (S) corresponds to the derivative of color-opponent mechanisms responses, and discrimination threshold ($1/S$) is plotted in function of φ in the computed hue discrimination curve (see App. B for computation details).

The HDC has been computed for stage 2 and stage 3 of Stockman and Brainard (2010) model [17] which is a version of the three-stage Müller zone model with updated spectral sensitivities, with stage 1 corresponding to Stockman and Sharpe (2000) cone-fundamentals (LMS) [18]. Stage 2 corresponds to L-M and S-(L+M) cone-opponent mechanisms and stage 3 to R/G ((S+L)-M) and a B/Y (S-(L+M)) color-opponent spectral mechanisms. Stage 2 is assimilated to discrimination mechanisms and stage 3 to color appearance mechanisms.

The HDC computed for the two stages (see Fig. 5) exhibits a periodical profile with two minima and two maxima occurring at 180° apart. It can be shown that this periodicity does not depend on frequency f nor amplitude m (see App. B). The difference between discrimination and appearance stages essentially lies in the 10° phase-shift in minima and maxima positions and in response amplitude. If theoretical HDCs correctly predict over the entire color circle the presence of two minima and two maxima as described on the empirical HDCs, they cannot predict the consistent non-opponent phases difference between the two minima for RB and VB. The first minima predicted at $90 - 100°$ between yellow and red categories is in agreement with the first minima found for VB and RB, whereas the second minima in the $270 - 280°$ located in the region of the blue/green boundary does not correspond to the empirical minima that, for the two observers, is located in the region of the blue/magenta boundary. Likewise, the predicted maximum of discrimination for green colors in the $180 - 190°$ corresponds to the region of lesser discrimination for VB and RB, but the predicted second maximum for lavender color at $0 - 10°$ does not match the second maximum observed for pink colors (30°). This non-opponent phase difference in the empirical HDC, although robust for our experimental conditions, will have to be confirmed. Alternatively, models including non-linear processes will need to be envisaged.

4.C. Discrimination minima and unique hues

Our initial question was to investigate possible relationship between discrimination performances and color appearance in relation to unique hues or color category boundaries. For the two observers, unique yellow and unique blue are located in close proximity with the unique blue-yellow line, but, and contrarily to Holtsmark & Valberg (1969) [6], their loci do not coincide with the two HDC minima. The absence of coincidence is further supported by the observers' verbal description of the stimuli eliciting these minima respectively named as blue and yellow mixed with a tinge of red. These results are consistent with Danilova & Mollon (2010) [5] findings. In their experiment, the authors probed unique hue loci and dis-

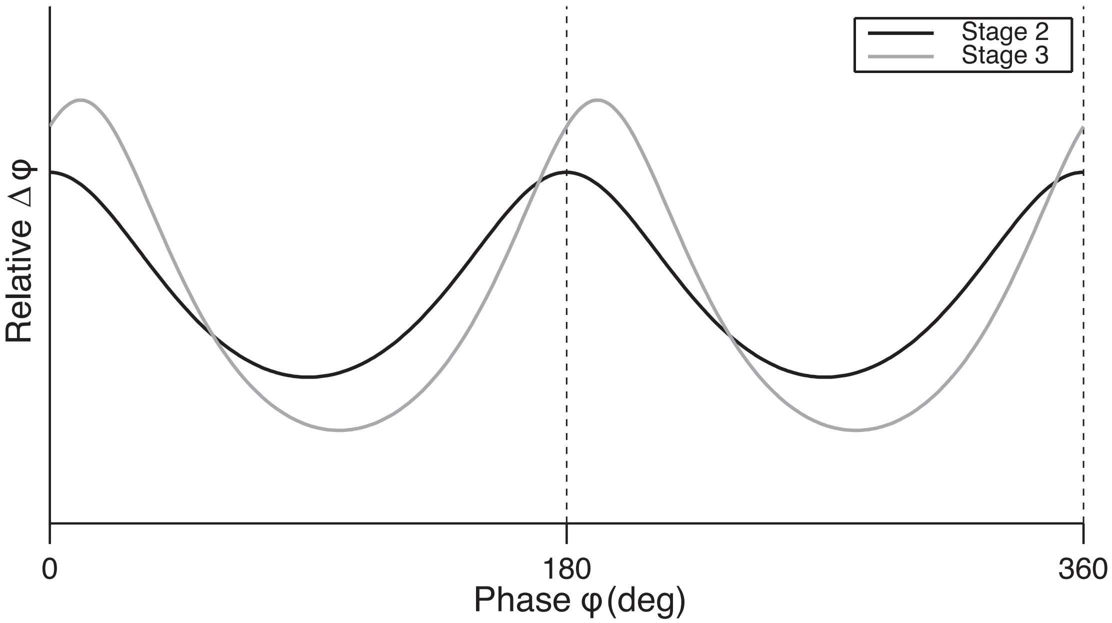

Fig. 5. Computed hue discrimination curve at stage 2 (black line) and at stage 3 (grey line) as proposed by Stockman & Brainard (2010) [17] (see Sec. 4.B for explanation).

crimination performances at different level of saturation along a predetermined unique blue (476 nm) -unique yellow (576 nm) line. Results showed an empirical unique hue line running parallel to the predetermined unique hue line. Minima of discrimination were located on a line parallel to the empirical unique hue line with an offset towards the +L direction.
Our results suggest that the smallest JND is obtained at the point where blue and yellow uniqueness brake down due to the detection of a red component, and consequently arises at two specified boundaries namely between yellow/orange and blue/magenta categories.

Unique green is associated with a poor discrimination region for which both, unique hue and discrimination threshold determinations required a high number of trials to optimize intra-observer variability. The minimum reported by Holtsmark & Valberg (1969) [6] with optimal color corresponding the blue/green boundary (located on the constant Munsell hue 10 BG curve) and associated to the wavelength discrimination curve 440 nm minima is absent from the empirical HDC. Experiments using CRT emulated Munsell colors reported a categorical perception effect as assessed by shorter reaction times at the blue /green category boundary suggesting a better discrimination at this boundary [19]. In experiments testing a restricted color gamut (i.e. two color categories), enhanced discrimination could result from a relative as opposed to an absolute minimum. To check for this possibility we looked at the HDC blue-green region. Based on the naming data, if 270° region is considered as the blue/green boundary for our two observers, greater phases correspond to the blue category, and yet are associated to smaller discrimination thresholds compared to phases straddling the category boundary. Consequently, no categorical perception effect for the blue/green boundary could be predicted from the HDC.

Although, data are limited to two observers, unique hue loci obtained with SSPDs are in good agreement with previous determinations obtained with monochromatic lights, color displayed on a monitor and color samples (see [20] for a comprehensive review of 10 studies). We already indicated that unique blue and unique yellow are close to the unique blue (476 nm) yellow (576 nm) line. In case of unique red, there are significantly less estimates due to the overlap with the non-spectral color region, yet with estimated λ_d of 599 and 619 nm, our determinations are in agreement with those reported by Kuehni (2004) [20]. Unique green loci with 529 nm (VB) and 550 nm (RB) are also in agreement with previous determinations, and the discrepancy between our two observers illustrates the classical inter-observer variability reported for this setting with a mean ranging from 506 to 544 nm [20]. However, difference between our two observers in the setting for unique green may well reflect shifts in the output of chromatic mechanisms as a result of age-related differences in the spectral absorption of short wavelength light by the lens [21].

Finally, unique hues are believed to correspond to the equilibrium state of a single R/G color-opponent mechanism for unique blue and unique yellow and to the equilibrium state of two Y/B color-opponent mechanisms for unique red and unique green [22]. The inspection of the sinusoidal spectral modulations that elicit unique blue and unique yellow is consistent with the existence of a single R/G appearance mechanism. With a frequency of 1.5 c at 317-320° (unique blue) and at 117-122° (unique yellow) such sinusoidal profiles exhibit a peak of energy at 473 nm and at 587-592 nm respectively. These energy peaks coincide almost perfectly with the nulling points (477 and 580 nm) of a R/G appearance mechanism as conceived in Stockman and Brainards model [17]. Peak of energy for sinusoidal profiles corresponding to unique green (196 and 220°) and unique red (76 and 79°) would in case of a single mechanism indicate nulling points located at 530 & 608 nm (VB) and 550 & 611 nm (RB) which is incompatible with the presence of a single zero-crossing along the wavelength axis reported for the Y/B mechanism.

Acknowledgments

Authors thank John Barbur for discussion on the manuscript.

References

1. S. Harnad, "Psychophysical and cognitive aspects of categorical perception: A critical overview," in "Categorical perception: The groundwork of cognition" , S. Harnad, ed. (Cambridge University Press, New York, 1987), chap. 1, pp. 1–52.
2. N. Smeulders, F. W. Campbell, and P. R. Andrews, "The role of delineation and spatial frequency in the perception of the colours of the spectrum," Vision Research **34**, 927–936 (1994).
3. K. A. Jameson, S. M. Highnote, and L. M. Wasserman, "Richer color experience in observers with multiple photopigment opsin genes," Psychonomic Bulletin & Review **8**, 244–261 (2001).
4. W. D. Wright and F. H. G. Pitt, "Hue-discrimination in normal colour-vision," Proceedings of the Physical Society **46**, 459–473 (1934).
5. M. V. Danilova and J. D. Mollon, "Parafoveal color discrimination: A chromaticity locus of enhanced discrimination," Journal of Vision **10**, Article 4, 1–9 (2010).
6. T. Holtsmark and A. Valberg, "Colour discrimination and hue," Nature **224**, 366–367 (1969).
7. H. Barlow, "What causes trichromacy? a theoretical analysis using comb-filtered spectra," Vision Research **22**, 635–643 (1982).
8. V. Bonnardel and F. J. Varela, "Color vision in the comb frequency domain," Biological Research **36**, 119–134 (2003).

9. V. Bonnardel and L. T. Maloney, “Daylight, biochrome surfaces, and human chromatic response in the fourier domain,” Journal of the Optical Society of America A **17**, 677–686 (2000).
10. Y. Mizokami, J. S. Werner, M. A. Crognale, and M. A. Webster, “Nonlinearities in color coding: Compensating color appearance for the eye’s spectral sensitivity,” Journal of Vision **6**, 996–1007 (2006).
11. V. C. Smith and J. Pokorny, “Chromatic-discrimination axes, CRT phosphor spectra, and individual variation in color vision,” Journal of the Optical Society of America A **12**, 27–35 (1995).
12. V. Bonnardel, H. Bellemare, and J. D. Mollon, “Measurements of human sensitivity to comb-filtered spectra,” Vision Research **36**, 2713–2720 (1996).
13. V. Bonnardel and E. M. Valero, “Study of colour discrimination with comb-filtered spectra,” Vision Research **41**, 541–548 (2001).
14. M. A. Webster, E. Miyahara, G. Malkoc, and V. E. Raker, “Variations in normal color vision. II. unique hues,” Journal of the Optical Society of America A **17**, 1545–1555 (2000).
15. M. A. Webster, S. M. Webster, S. Bharadwaj, R. Verma, J. Jaikumar, G. Madan, and E. Vaithilingham, “Variations in normal color vision. III. unique hues in indian and united states observers,” Journal of the Optical Society of America A **19**, 1951–1962 (2002).
16. H. Sun, H. E. Smithson, Q. Zaidi, and B. B. Lee, “Specificity of cone inputs to macaque retinal ganglion cells,” Journal of Neurophysiology **95**, 837–849 (2006).
17. A. Stockman and D. H. Brainard, “Color vision mechanisms,” in “Handbook of Optics, Third Edition Volume III: Vision and Vision Optics” , M. Bass, C. DeCusatis, J. Enoch, V. Lakshminarayanan, G. Li, C. MacDonald, V. Mahajan, and E. V. Stryland, eds. (McGraw-Hill Professional, 2010), chap. 11, pp. 11.1–11.104, 3rd ed.
18. A. Stockman and T. L. Sharpe, “The spectral sensitivities of the middle- and long-wavelength-sensitive cones derived from measurements in observers of known genotype,” Vision Research **40**, 1711–1737 (2000).
19. A. L. Gilbert, T. Regier, P. Kay, and R. B. Ivry, “Whorf hypothesis is supported in the right visual field but not the left,” Proceedings of the National Academy of Sciences of the United States of America **103**, 489 –494 (2006).
20. R. G. Kuehni, “Variability in unique hue selection: A surprising phenomenon,” Color Research & Application **29**, 158–162 (2004).
21. J. van de Kraats and D. van Norren, “Optical density of the aging human ocular media in the visible and the UV,” Journal of the Optical Society of America A **24**, 1842–1857 (2007).

22. S. M. Wuerger, P. Atkinson, and S. Cropper, “The cone inputs to the unique-hue mechanisms,” Vision Research **45**, 3210–3223 (2005).

A. Appendix A: Modeling SSPD

The illumination modulation functions is defined as:

$$E_\varphi(\lambda) = 1 + m\sin(p(f(1.2\lambda + 480) + \varphi)) \tag{1}$$

In the model, we consider the SSPDs measured at the output of the integrating sphere (see Sec.2).

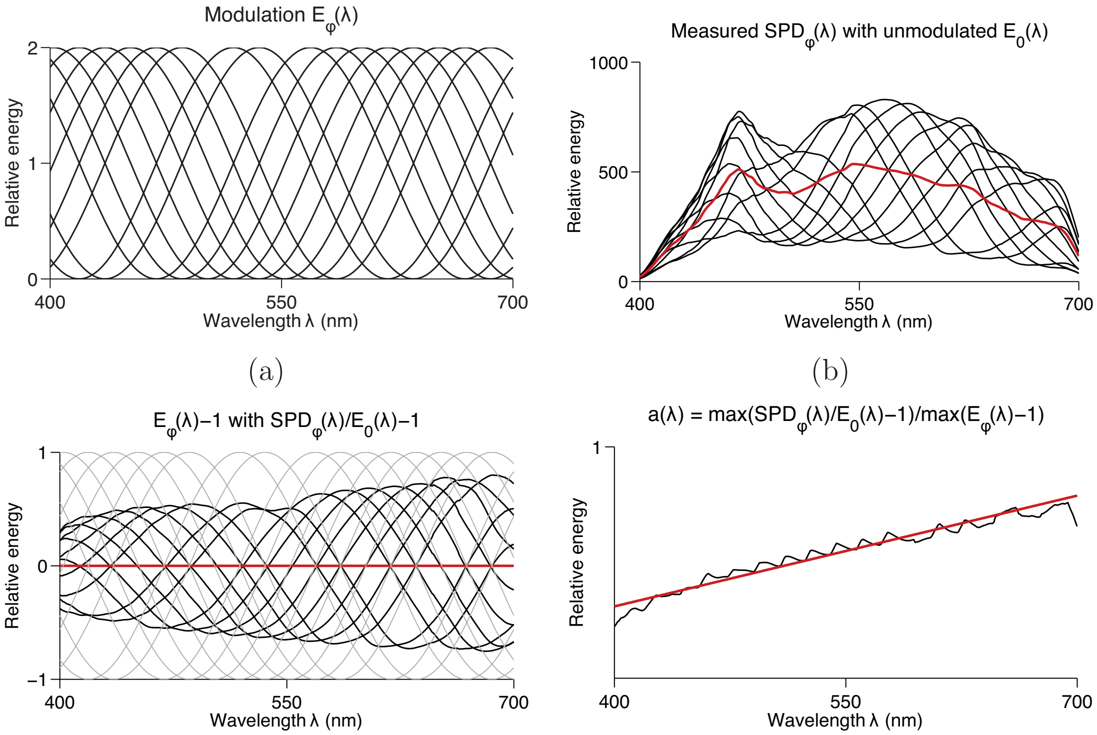

(a) (b)

(c) (d)

Fig. A. (Color online) (a) Electronic mask profiles (b) Measured SPDs $SPD_\varphi(\lambda)$ (black lines) and measured unmodulated light E_0 (thick grey line) (c) $(SPD_\varphi(\lambda)/E_0(\lambda)) - 1$ (black lines) compared to the electronic mask profiles (grey lines) (d) Estimated gain function $a(\lambda)$ (black line) and its linear approximation $A(\lambda)$ (thick grey line).

Thus, we applied the modulation $E_\varphi(\lambda)$ on the unmodulated SPD $E_0(\lambda)$. Fig. A(a) shows the sinusoidal electronic mask profiles displayed on the LCD. For a phase φ, Fig. A(b) shows the resulting SSPD measures, noted $SPD_\varphi(\lambda)$. Fig. A(c) shows the electronic mask profiles and those corresponding to the ratio $(SPD_\varphi(\lambda)/E_0(\lambda))-1$. It can be seen that the two types of profile are different. Their differences, or gain, vary with wavelength and is noted $a(\lambda)$

(see Fig. A(d)). Its linear approximation function $A(\lambda)$ (red line) is included in the model now expressed as:

$$SPD_{\varphi}(\lambda) = A(\lambda)E_0(\lambda)(E_{\varphi}(\lambda) - 1) + E_0(\lambda) \tag{2}$$

B. Appendix B: Chromatic opponency coding as a linear model

B.A. Determination of LMS responses to SSPD

The LMS cone responses to the SSPDs are defined by the following equation:

$$\left\{ \begin{array}{rcl} L(\varphi) & = & \int_{\lambda} L(\lambda) SPD_{\varphi}(\lambda) d\lambda \\ M(\varphi) & = & \int_{\lambda} M(\lambda) SPD_{\varphi}(\lambda) d\lambda \\ S(\varphi) & = & \int_{\lambda} S(\lambda) SPD_{\varphi}(\lambda) d\lambda \end{array} \right. \tag{3}$$

From Eq.(1) and Eq.(2) we have:

$$\begin{aligned} E_{\varphi}(\lambda) &= 1 + m \sin\left(\underbrace{pf\,(1.2\lambda + 480)}_{a} + \underbrace{p\varphi}_{\Phi} \right) \\ &= 1 + m \sin(a)\cos(\Phi) + m \sin(\Phi)\cos(a) \\ SPD_{\varphi}(\lambda) &= A(\lambda)E_0(\lambda)\left(E_{\varphi}(\lambda) - 1\right) + E_0(\lambda) \\ &= E_0(\lambda) \\ &\quad + m \sin(a)\cos(\Phi)A(\lambda)E_0(\lambda) \\ &\quad + m \sin(\Phi)\cos(a)A(\lambda)E_0(\lambda) \end{aligned}$$

From Eq.(3), because φ and λ are independent variables we can write:

$$\begin{aligned} L(\varphi) &= \underbrace{\int_{\lambda} E_0(\lambda)L(\lambda)d\lambda}_{A_L} \\ &\quad + \cos(\Phi)\, \underbrace{m \int_{\lambda} A(\lambda)E_0(\lambda)\sin(a)L(\lambda)d\lambda}_{C_L} \\ &\quad + \sin(\Phi)\, \underbrace{m \int_{\lambda} A(\lambda)E_0(\lambda)\cos(a)L(\lambda)d\lambda}_{D_L} \\ &= A_L + C_L\cos(\Phi) + D_L\sin(\Phi) \end{aligned}$$

Which could be written (see following Proof):

$$\begin{aligned} L(\varphi) &= A_L + B_L \sin(\Phi + K_L) \quad \text{with:} \\ B_L &= \sqrt{C_L^2 + D_L^2} \quad \text{and} \quad K_L = \arctan\left(\frac{C_L}{D_L}\right) \end{aligned}$$

Proof:

$$A\cos x + B\sin x = C\sin(x+p) \text{ with } C = \sqrt{A^2+B^2} \text{ and } p = \arctan\left(\frac{A}{B}\right)$$

$$\begin{aligned} A\cos x + B\sin x &= C\sin(x+p) \\ A\cos x + B\sin x &= C\sin x\cos p + C\cos x\sin p \end{aligned}$$

because $\sin(a+b) = \sin a\cos b + \cos a\sin b$, thus by identification of the two sides of the equation:

$$\left\{\begin{array}{lcl} A &=& C\sin p \\ B &=& C\cos p \end{array}\right. \Leftrightarrow \left\{\begin{array}{lcl} A^2+B^2 &=& C^2\underbrace{(\sin^2 p + \cos^2 p)}_{=1} \\ \frac{A}{B} &=& \frac{\sin p}{\cos p} = \tan p \end{array}\right. \Leftrightarrow \left\{\begin{array}{lcl} C &=& \sqrt{A^2+B^2} \\ p &=& \arctan\left(\frac{A}{B}\right) \end{array}\right.$$

end proof.△

Thus, $L(\varphi)$, $M(\varphi)$ and $S(\varphi)$ function responses (see Fig. B) to the stimulation $E_\varphi(\lambda)$ are sinusoid functions (thus derivable) defined as:

$$\left\{\begin{array}{lcl} L(\varphi) &=& A_L + B_L\sin(\Phi + K_L) \\ M(\varphi) &=& A_M + B_M\sin(\Phi + K_M) \\ S(\varphi) &=& A_S + B_S\sin(\Phi + K_S) \end{array}\right. \tag{4}$$

$$\begin{aligned} &\text{with for } i \in \{L, M, S\} \\ A_i &= \int_\lambda E_0(\lambda) i(\lambda) d\lambda \\ B_i &= m\sqrt{C_i^2 + D_i^2} \\ K_i &= \arctan\left(\frac{C_i}{D_i}\right) \\ C_i &= m\int_\lambda A(\lambda)E_0(\lambda)\sin(a) i(\lambda) d\lambda \\ D_i &= m\int_\lambda A(\lambda)E_0(\lambda)\cos(a) i(\lambda) d\lambda \\ &\text{and} \\ a &= pf\,(1.2\lambda - 480)\,, \quad \Phi = p\varphi, \quad p = \frac{2\pi}{360} \end{aligned}$$

B.B. *Determination of ATD responses to SSPD*

With an opponent chromatic coding, Eq.(4) response functions of LMS cones are transformed into opponent chromatic channels called $A(\varphi)$, $T(\varphi)$ and $D(\varphi)$ through a linear transform.

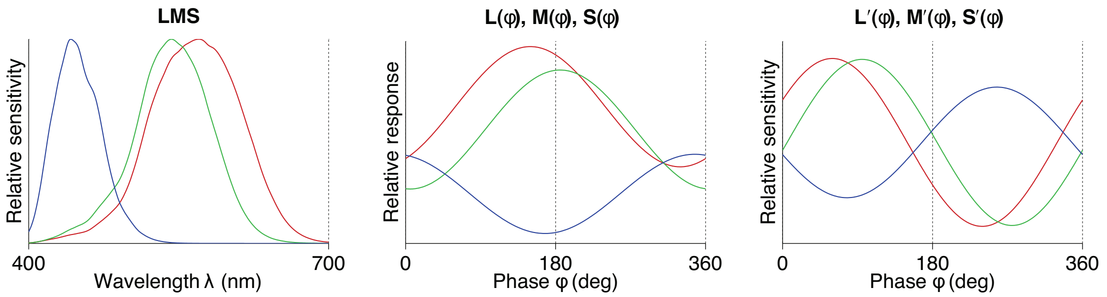

(a) (b) (c)

Fig. B. (Color online) (a) Stockman & Sharpe (2000) 2° cone spectral sensitivities [18], $L(\lambda)$, $M(\lambda)$ and $S(\lambda)$. (b) Response function calculated with Eq.(4), $L(\varphi)$, $M(\varphi)$ and $S(\varphi)$. (c) Derivative functions corresponding to sensitivity threshold, $L'(\varphi)$, $M'(\varphi)$ and $S'(\varphi)$.

If we called $\mathbf{Y}(\varphi)$ the corresponding vector in the ATD opponent space, we have:

$$\underbrace{\begin{bmatrix} A(\varphi) \\ T(\varphi) \\ D(\varphi) \end{bmatrix}}_{\mathbf{Y}(\varphi)} = \underbrace{\begin{bmatrix} n_{11} & n_{12} & n_{13} \\ n_{21} & n_{22} & n_{23} \\ n_{31} & n_{22} & n_{33} \end{bmatrix}}_{\mathbf{M}} \underbrace{\begin{bmatrix} L(\varphi) \\ M(\varphi) \\ S(\varphi) \end{bmatrix}}_{\mathbf{X}(\varphi)} \tag{5}$$

By analogy with Sec. B.A, Eq.(5) response functions, $A(\varphi)$, $T(\varphi)$ and $D(\varphi)$ (see Fig. C), to the stimulation $E_\varphi(\lambda)$ are sinusoid functions.

B.C. A model including opponent chromatic coding

The opponent vector $\mathbf{Y}(\varphi)$ and its derivative along φ expressed as the vector of LMS response, $\mathbf{X}(\varphi)$, write:

$$\mathbf{Y}(\varphi) = \mathbf{M}\mathbf{X}(\varphi),\ \mathbf{Y}'(\varphi) = \mathbf{M}\mathbf{X}'(\varphi) \tag{6}$$

If we consider that the threshold is measured in $\mathbf{Y}$ space as the inverse of sensitivities of the ATD mechanisms. We suppose that sensitivities are estimated from a square metric and that the variation of the signal is small enough to consider derivative along φ of the adapted opponent chromatic responses instead of the signal itself. We write:

$$(\Delta\varphi)^2 = \frac{1}{\mathbf{Y}'(\varphi)^T\mathbf{Y}'(\varphi)} = \frac{1}{\mathbf{X}'(\varphi)^T\mathbf{M}^T\mathbf{M}\mathbf{X}'(\varphi)} \tag{7}$$

According to Eq.(4) and Eq.(5), $\mathbf{X}'(\varphi)$ could be written:

$$\begin{aligned}
\mathbf{X}'(\varphi) &= \begin{bmatrix} pB_L \cos(p\varphi + K_L) \\ pB_M \cos(p\varphi + K_M) \\ pB_S \cos(p\varphi + K_S) \end{bmatrix} \\
&= \begin{bmatrix} pB_L \cos(p\varphi)\cos(K_L) - pB_L \sin(p\varphi)\sin(K_L) \\ pB_M \cos(p\varphi)\cos(K_M) - pB_M \sin(p\varphi)\sin(K_M) \\ pB_S \cos(p\varphi)\cos(K_S) - pB_S \sin(p\varphi)\sin(K_S) \end{bmatrix} \\
&= p\cos(p\varphi) \underbrace{\begin{bmatrix} B_L \cos(K_L) \\ B_M \cos(K_M) \\ B_S \cos(K_S) \end{bmatrix}}_{\mathbf{I}} - p\sin(p\varphi) \underbrace{\begin{bmatrix} B_L \sin(K_L) \\ B_M \sin(K_M) \\ B_S \sin(K_S) \end{bmatrix}}_{\mathbf{J}} \\
\mathbf{X}'(\varphi) &= p\cos(p\varphi)\mathbf{I} - p\sin(p\varphi)\mathbf{J}
\end{aligned}$$

Thus,

$$\begin{aligned}
\mathbf{X}'(\varphi)^T\mathbf{M}^T\mathbf{M}\mathbf{X}'(\varphi) &= \left(p\cos(p\varphi)\mathbf{I} - p\sin(p\varphi)\mathbf{J}\right)^T \mathbf{M}^T\mathbf{M} \left(p\cos(p\varphi)\mathbf{I} - p\sin(p\varphi)\mathbf{J}\right) \\
&= p^2(\cos(p\varphi))^2\mathbf{I}^T\mathbf{M}^T\mathbf{M}\mathbf{I} \\
&\quad -p^2\cos(p\varphi)\sin(p\varphi)(\mathbf{I}^T\mathbf{M}^T\mathbf{M}\mathbf{J} + \mathbf{J}^T\mathbf{N}^T\mathbf{N}\mathbf{I}) \\
&\quad +p^2(\sin(p\varphi))^2\mathbf{J}^T\mathbf{M}^T\mathbf{M}\mathbf{J} \\
&\quad \text{which could be written using proof below} \\
\mathbf{X}'(\varphi)^T\mathbf{M}^T\mathbf{M}\mathbf{X}'(\varphi) &= A + B\cos(2p\varphi + K) \qquad (8)
\end{aligned}$$

Finally, combination of Eq.(7) and Eq.(8) gives:

$$\begin{aligned}
\Delta\varphi &= \frac{1}{\sqrt{A + B\cos(2p\varphi + K)}} \\
&\quad \text{with} \\
A &= \frac{p^2}{2}(C + F),\ B = \frac{p^2}{2}\sqrt{(C - F)^2 + (D + E)^2} \\
K &= \arctan\left(\frac{D + E}{C - F}\right) \\
C &= \mathbf{I}^T\mathbf{M}^T\mathbf{M}\mathbf{I} \\
D &= \mathbf{I}^T\mathbf{M}^T\mathbf{M}\mathbf{J} \\
E &= \mathbf{J}^T\mathbf{M}^T\mathbf{M}\mathbf{I} \\
F &= \mathbf{J}^T\mathbf{M}^T\mathbf{M}\mathbf{J} \qquad (9)
\end{aligned}$$

The model of threshold prediction using second or third stage opponent chromatic coding is thus linear and can be expressed as the inverse of the square of a sinusoidal function. Fig. 5 shows computed hue discrimination curves for second and third stage opponent models as proposed by Stockman and Brainard (2010) [17].

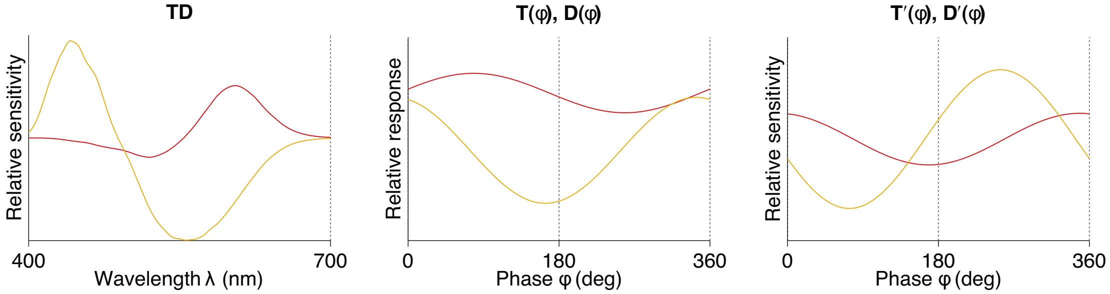

(a) (b) (c)

Fig. C. (Color online) (a) Spectral sensitivities $T(\lambda) = L(\lambda) - M(\lambda)$ and $D(\lambda) = S(\lambda) - 0.69 \times (L(\lambda) + 0.5 \times M(\lambda))$. (b) Response function calculated with Eq.(5), $T(\varphi)$ and $D(\varphi)$. (c) Derivative functions corresponding to sensitivity threshold, $T'(\varphi)$ and $D'(\varphi)$.